

Student Symposium

Wednesday, June 21

Session I

S1

REAL STRUCTURE OF FERRITIC STEEL AND FERRITE PHASE OF DUPLEX STEEL AFTER ROLLING

J. Čapek, K. Trojan, J. Němeček, N. Ganev

Department of Solid State Engineering, Faculty of Nuclear Sciences and Physical Engineering,
Czech Technical University in Prague

jiri.capek@jfifi.cvut.cz

Duplex stainless steels have high corrosion resistance in many environments, where the standard austenitic and ferritic steel is consumed and where their properties significantly exceed single phase steel. Duplex steels combine properties of both phases and due to two-phase microstructure, some properties are better than high-alloyed single-phase steel, e.g. abrasion resistance [1]. Thereby, smaller amount of material from duplex steel is necessary to manufacture function components. Duplex steels are due to austenite phase susceptible to mechanical reinforcement, i.e. local changes in mechanical properties of surface layers.

The importance of the texture resides in the anisotropy of most material properties. For this reason, the determination and subsequent interpretation of the texture in material engineering is very important. Moreover, texture analysis during the thermo-mechanical processing of materials provides information on basic mechanisms including deformation, recrystallization or phase transformation. The properties, which are influenced, are, for example, the Young's modulus of elasticity, Poisson number, hardness, strength, ductility, abrasion resistance, magnetic permeability, electrical conductivity etc. So called plastic aniso-

tropy prefer to use a certain slide plane system during deformation. Texture is therefore used in the production of materials with specific properties [2]. Major deformation mechanisms responsible for the formation of ferrite and austenite rolling textures in duplex steels should be the same as in the single phase steels; however their contribution and significance are expected to change [3].

Generally, metals and alloys with a body centred cubic lattice (bcc) tend to form fibre textures. For bcc material, there are six characteristic fibres [4]. Most orientations are formed into two characteristic fibres of Euler space. During cold rolling, primarily, the α_1 and α_2 fibre are created. The α_1 fibre is characterized by crystallographic direction $\langle 110 \rangle$ which is parallel to rolling direction, e.g. $\{001\}\langle 110 \rangle$, $\{112\}\langle 110 \rangle$, $\{111\}\langle 110 \rangle$. The α_2 fibre include crystallographic directions with $\{111\}$ planes which are parallel to normal direction, e.g. $\{111\}\langle 110 \rangle$, $\{111\}\langle 112 \rangle$ [2, 3, 5]. The values of texture components are significantly dependent on the structure (especially on the grain size and initial texture), chemical and phase composition [3].

The tested samples of plate shape were made of AISI 420 (ferritic) and AISI 318LN (duplex) type of stainless

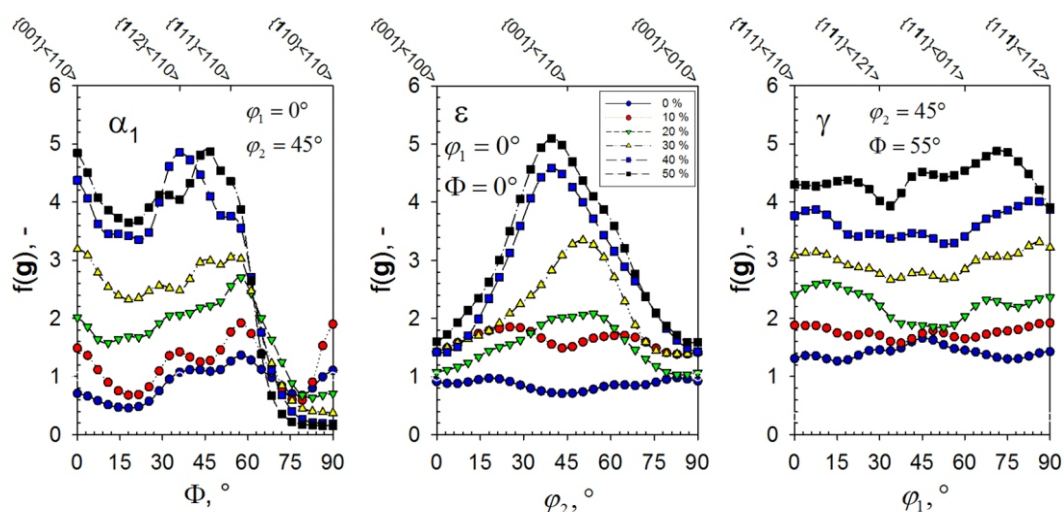


Figure 1. Values of ODF, i.e. $f(g)$, along α_1 , ϵ , and γ fibres of ferritic steel.



steel. The samples were rolled with 0, 10, 20, 30, 40, and 50% reduction of thickness. At the end, the samples were annealed in air laboratory furnace for 7 hours at 650 °C in order to reduce residual stresses.

Using CoK radiation, X'Pert PRO MPD diffractometer was used to sample analysis. Texture analysis was performed on the basis of the orientation distribution function (ODF) calculated from experimental pole figures recorded of three planes $\{110\}/\{220\}$, $\{200\}$, and $\{211\}$ using MTEX software.

According to [3], after 40% of deformation the limited ρ_{110} and ρ_{200} fibres, see Fig. 1, may describe the rolling texture of ferrite. It is evident that initial texture (0% deformation) is nearly random. For higher degree of deformation, ρ_{110} and ρ_{200} fibres are dominant components of rolling texture of ferritic steel. Ferritic steel exhibited the $\{001\}\langle 110\rangle$, $\{112\}\langle 110\rangle$, and $\{111\}\langle 110\rangle$ orientations which are components of ρ_{110} fibre texture. Rotated cubic orientation $\{001\}\langle 110\rangle$ is one of the typical components of ferrite rolling texture. All fibres assume the higher values of the ODF for increasing degree of deformation. Both fibres ρ_{110} and ρ_{200} describing the final texture are very inhomogeneous.

Nevertheless, it is necessary to expect that two-phase steel have different behaviour of the constituent phases in comparison with single-phase steel [6]. In most cases, there will be differences between the textures of two- and single-phase steels. According to [3], these values of fibres are not typical for ferrite phase in duplex steels.

1. R. Dakhlaoui, C. Braham, A. Baczański, *Mater. Sci. Eng.: A*, 70.1, (2007), 6-17.
2. H. J. Bunge, *Texture Analysis in Materials Science*. London: Butterworth. 1982.
3. J. Ryš, W. Ratuszek, M. Witkowska, *Arch. Metall. Mater.*, 50.3, (2006), 495-502.
4. S. Suwas, R. K. Ray, *Crystallographic Texture of Materials*. Springer-Verlag. 2014.
5. H. Hu, *Texture*, 1.4, (1974), 233-258.
6. J. Čapek, K. Kolařík, Z. Pitrmuc, L. Beránek, N. Ganev, *Material Structure*, 23, 4, (2016), 362-363.

This work was supported by the Grant Agency of the Czech Technical University in Prague, grant No. SGS16/245/OHK4/3T/14.

S2

THE $\{110\}$ -NANOTWINNED PHASE IN THE VICINITY OF THE MARTENSITIC TRANSFORMATION IN Ni-Mn-Ga

P. Veřtát^{1,2}, L. Straka², J. Drahokoupil^{1,2}, O. Heczko²

¹Department of Solid State Engineering, FNSPE CTU in Prague, Trojanova 13, 120 00, Prague 2, Czech Republic

²Department of Advanced Structural Materials, Institute of Physics of the Czech Academy of Sciences, Na Slovance 2, 182 21 Praha 8, Czech Republic
vertapet@fjfi.cvut.cz

Martensite of the Ni-Mn-Ga magnetic shape memory Heusler alloys exhibits large magnetoelastic response and it is, therefore, of current interest for possible applications in actuator and magnetocaloric devices. The primary condition for the magnetic shape memory effect is a phase transformation from the high temperature and high symmetry cubic austenite to a low symmetry martensite phase. We focus on the non-stoichiometric compositions of the Ni-Mn-Ga resulting in modulated 10M martensitic structure.

Apart from the well-known martensitic transformation observable e.g. as a steep change in the AC magnetic susceptibility, electric resistivity and dilatation curves [1], we recently discovered a non-standard behaviour of the temperature dependence of electric resistivity, few tenths of kelvin below the transformation to austenite (Fig. 1). Similar effect on the evolution of the lattice parameters was observed by Richterová [2] making the initial set of measurements.

We measured the temperature evolution of the lattice parameters of single-crystalline samples with very fine temperature step, using the PANalytical X'Pert PRO diffractometer and Peltier element for heating [3]. The divergent geometry and the twinned microstructure allow us

to observe the 400 and 040 reflections simultaneously in one relatively quick (~ 20 s) scan with reasonable resolution (Fig. 2). Very slow heating (0.8 K/min or lower) allows us to observe this dynamic effect in detail.

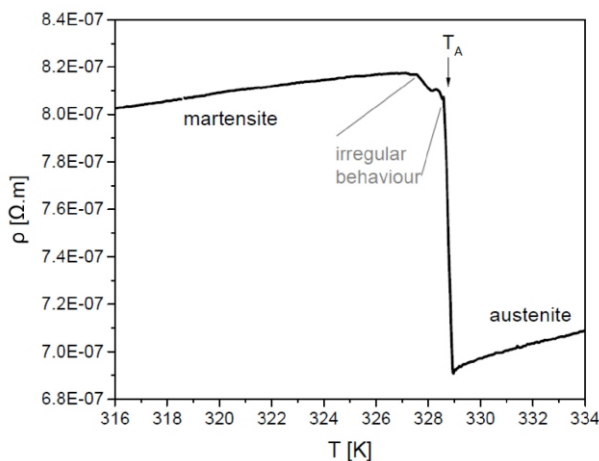


Figure 1. Electric resistivity as the function of temperature. Linear evolution during heating in martensite followed by irregular behaviour before the steep jump to austenite at T_A .

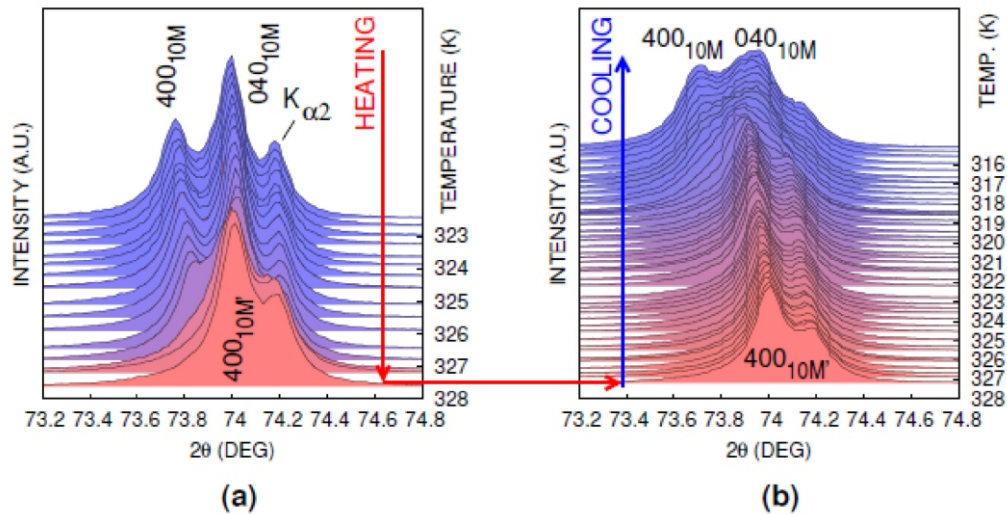


Figure 2. 400 and 040 reflections as a function of temperature (background level corresponds to temperature on the right axis) upon heating (a) and cooling (b). [4]

In the temperature region analogous to the irregular region in the resistivity measurement, two reflections 400 and 040 of the original 10M martensite merged to one peak of the new phase marked as 10M'. This structural change prior transformation to austenite corresponds to changes in resistivity shown in Fig. 1. The heating was stopped just below the T_A and immediately followed by cooling resulting in observable hysteresis of the occurrence of the 10M' phase, as seen in Fig. 2.

Measured data were fitted in custom-made program based on *MS Excel* and *VBA for applications*, using *solver.xlam* add-in for the least squares method implementation. Four parameters of the pseudo-Voigt function used for each profile fitting were obtained – intensity at maximum, 2θ position, relative width and shape parameter [5]. Thermal evolution of the calculated lattice parameters a and b of the 10M phase and the a' parameter of the 10M' phase and corresponding maximal intensities of the diffraction lines during heating are shown in Fig. 3-4.

Although the 10M' phase seems to be present in the whole temperature interval, the intensity of the corresponding reflection before transition to 10M' is approximately

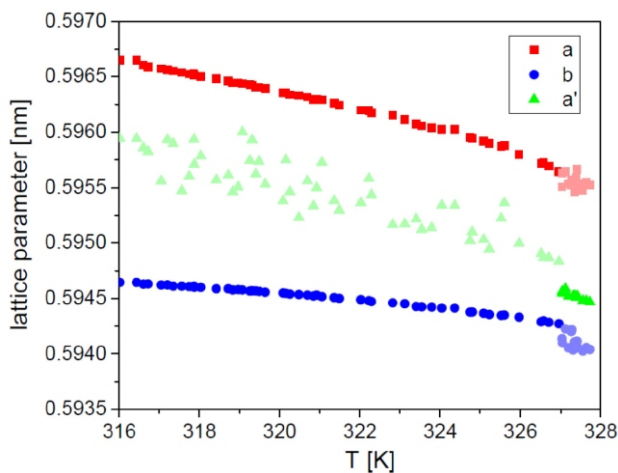


Figure 3. Development of the lattice parameters a and b of the 10M and a' of the 10M' structure during heating. Dominant phase is marked with more saturated colour.

two orders lower than the intensity of the reflections corresponding to the dominant 10M phase. Therefore, the lattice parameter a' in lower temperature region can only be estimated with major errors and is depicted just to complete the overall image. As the lattice parameter of austenite is far from depicted region ($a_a = 0.584$ nm at $T = 332$ K), the 10M' phase cannot be ascribed to austenite.

Upon cooling, the 10M' phase remains stable in a broader temperature interval, then it transforms back to 10M structure at ~ 318 K. The reciprocal space mapping showed no significant difference between the 10M and 10M' – in particular, the same satellite reflections were present in the maps.

After the theoretical calculations of the diffraction lines and detailed scanning electron microscopy (SEM) observations, the 10M' was ascribed to be the $\{110\}$ -nanotwinned form of the 10M monoclinic phase originating from the low energy of the a/b twin boundaries (see ref. [4] for details).

1. P. Veřtát, J. Drahokoupil, O. Perevertov, O. Heczko, *Phase Transitions*, **89**, (2016), pp. 752-760.

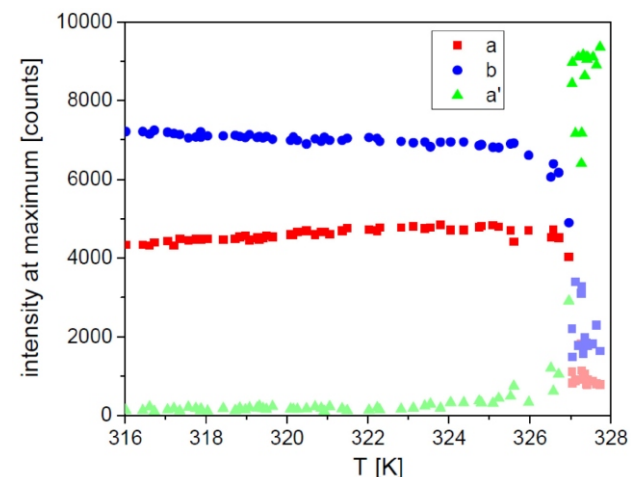


Figure 4. Intensities of the diffraction lines during heating corresponding to Fig. 3.



2. K. Richterová, J. Drahokoupil, O. Heczko, *Materials Structure*, **20**, (2013), pp. 108-110.
3. J. Drahokoupil, *Materials Structure*, **22**, (2015), pp. 164-165.
4. L. Straka, J. Drahokoupil, P. Veřtát, J. Kopeček, M. Zelený, H. Seiner, O. Heczko, *Acta Mater.*, **132**, (2017), pp. 335-344.
5. R. Kužel, *Materials Structure*, **10**, (2003), pp. 18-19.

This work was supported by the Grant Agency of the Czech Technical University in Prague, grant No. SGS16/245/OHK4/3T/14.

S3

XRD ON A HIGH ENTROPY ALLOY

Martin Dudr^{1,2}, František Lukáč²

¹*Department of Solid State Engineering, Faculty of Nuclear Sciences and Physical Engineering Czech Technical University in Prague, Trojanova 13 120 00 Prague 2, Czech Republic*

²*Institute of plasma physics, Za Slovankou 1782/3 182 21 Prague, Czech Republic*

martin.dudr@gmx.com

High Entropy Alloys (HEAs) are multicomponent alloys defined by being comprised of at least five elements in equiatomic or near-equiatomic ratios (that is usually interpreted as a range of 5-35 at.% per element). High configurational entropy of these alloys may enhance the formation of one equilibrium phase as solid solution with randomly distributed atoms occupying lattice points of usually BCC or FCC structure.

The special nature of these alloys allows them to have remarkable properties like high hardness, stability of phase composition, creep resistance, radiation resistance, low diffusion coefficient, biocompatibility and others.

The Hf-Nb-Ta-Ti-Zr alloy (HfNbTaTiZr) has been developed as a refractory alloy by Senkov in 2011. [1] It is also considered as a potential biocompatible material. [2] It forms a single phase BCC solid solution at RT.

Several ingots of this alloy have been prepared using the arc melting method in protective argon atmosphere by UJP s.r.o. company and they are being analysed using various methods, XRD being one of them. During preparation the alloy was melted and mixed in a copper crucible which was water-cooled at the bottom. Different cooling conditions in different places of the crucible resulted in nonhomogenous microstructure in the as-cast ingot. Samples were cut out transversely from the ingot bar and were analysed by XRD, SEM and optical microscopy.

Rietveld refinement was used (Fundamental Parameters Approach in TOPAS V5 software [3,4]) to determine

the lattice parameter, size of coherently diffracting domains and microstrains from the XRD measurements.

The cross section of the ingot revealed both dendritic microstructure and big grains – the first mentioned was located near the free surface and the second near the bottom of cooled crucible. This heterogeneous microstructure caused large differences between XRD patterns obtained from different regions of the sample.

Special attention was dedicated to the investigation of thermal stability of the alloy up to 1400°C during in situ annealing in XRD high temperature chamber. So far the decomposition of the BCC solid solution into two BCC solutions with similar lattice parameter at cca 900°C has been observed at high-temperature XRD measurement. More measurements are to be carried out at HTXRD and also at DSC to understand better the behaviour of the alloy.

1. O.N. SENKOV, J.M. SCOTT, S.V. SENKOVA, D.B. MIRACLE, C.F. WOODWARD, *Journal of Alloys and Compounds*, **509:20**, (2011), pp. 6043–48.
2. V. BRAIC, M. BALACEANU, M. BRAIC, A. VLADESCU, S. PANSERI, A. RUSSO, *J Mech Behav Biomed Mate.*, **10**, (2012), pp. 197-205.
3. R.W. CHEARY, A. COELHO, *J. Appl. Crystallogr.*, **25:2**, (1992), pp. 109–121.
4. A. A. COELHO, TOPAS version 5 (Computer Software), Coelho Software, Brisbane, (2016).

REAL STRUCTURE AND RESIDUAL STRESSES IN ADVANCED WELDS DETERMINED BY X-RAY AND NEUTRON DIFFRACTION ANALYSIS

K. Trojan¹, J. Čapek¹, Ch. Hervoches², N. Ganev¹, P. Mikula², K. Kolařík¹

¹CTU in Prague, Department of Solid State Engineering, Faculty of Nuclear Sciences and Physical Engineering, Trojanova 13, 120 00 Prague 2, Czech Republic

²Nuclear Physics Institute, ASCR, v.v.i., Department of Neutron Physics, 25068 Řež, Czech Republic
Karel.Trojan@jfifi.cvut.cz

Laser processing is nowadays widely used in modern industry, mainly because of its high productivity and precision. Developed laser welding methods using high power lasers took over the capability to fill groove with cold or hot wire metal from arc welding. This leads to change in mechanical properties of welds, especially reducing their hardness due to the quenching [1]. Therefore, the paper outlines using X-ray and neutron diffraction the capability of the advanced laser welding for joining thick sheets of structural steel in comparison with arc welding specifically metal active gas (MAG) welding. Profitable changes of real crystallographic structure and residual stresses (RS) in comparison with conventional laser welds improve the results during impact and tensile test and mainly enhance fatigue life. This has been shown in the article [2]. This paper describes the effects of welding on the RS and the real crystallographic structure (phase composition, crystallite size, microstrain) on cross-section of welds. Furthermore, the results of neutron diffraction verify previous assumptions of RS redistribution as a result of the surface preparation for determination measured lines by X-ray diffraction in two directions on the cross-section of the welds.

The analysed butt-welds were prepared by a double sided laser welding with cold wire and multilayer double side MAG welding from two $300 \times 150 \times 20$ mm³ sheets made of S355J2 steel. The measurements were performed in three lines perpendicular to the welds. One line passes through the centre of the weld and the other two are located three millimetres below each surface. The example of comparison of RS for upper line obtained by neutron and X-ray diffraction in direction perpendicular to the weld is plotted for both samples in Fig. 1. In addition, phase analyses were

measured on the cross sections, where the weight representation of retained austenite (see Fig. 2), crystallite size and microstrain (see Fig. 3) were evaluated by Rietveld analysis. In the graphs, the centre of the welds is given by zero on the x-axis.

The resulting RS gradients obtained using both methods with a different approach are in clear correlation. The redistribution of RS during the cutting has not yet been accurately described, but it can be deduced from these presented results that the preparation of the cross-section for X-ray diffraction measurements of the welds did not significantly change the distribution of residual stresses in the cutting plane. They were only partially affected. The dependency of retained austenite for the laser weld copies the boundary between the melt pool and the HAZ where the cooling was the fastest. On the contrary, the microstrain reaches the highest values in the middle of the original melt pool.

From our point of view, X-ray diffraction is a suitable instrument to describe the real structure and residual stress state even for the cross-section of such thick plates. However, it is necessary to keep in mind that even the residual stresses in the plane of the cut are partially affected by preparing the cross-section. It is often assumed that the residual stresses in this plane are not affected, but it is not always the correct assumption even according to these results.

1. M. Sokolov, A. Salminen, M. Kuznetsov, I. Tsubulskiy, *Materials & Design*, **32**, (2011), pp. 5127-5131.
2. I. Černý, & J. Sis, *Key Engineering Materials*, **713**, (2016), pp 82-85.

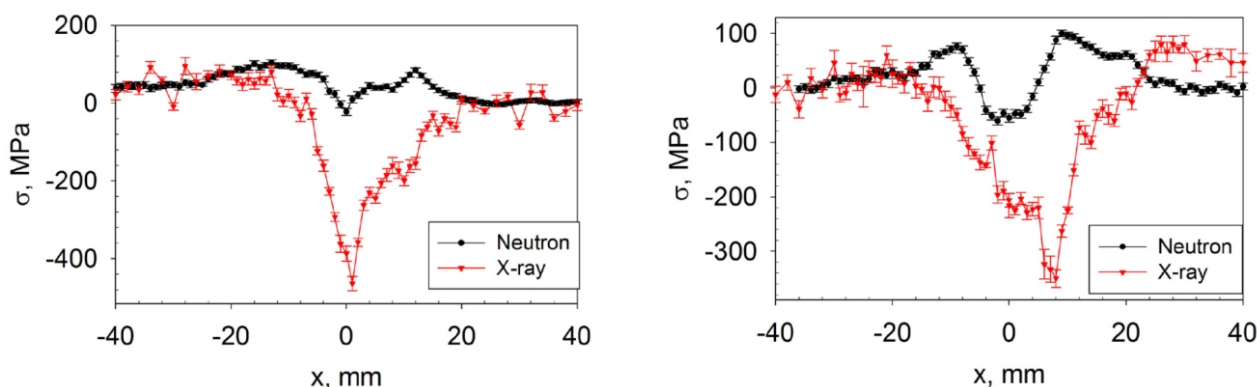


Figure 1. Comparison of RS obtained by X-ray and neutron diffraction in direction perpendicular to the weld for laser (left) a MAG sample (right).

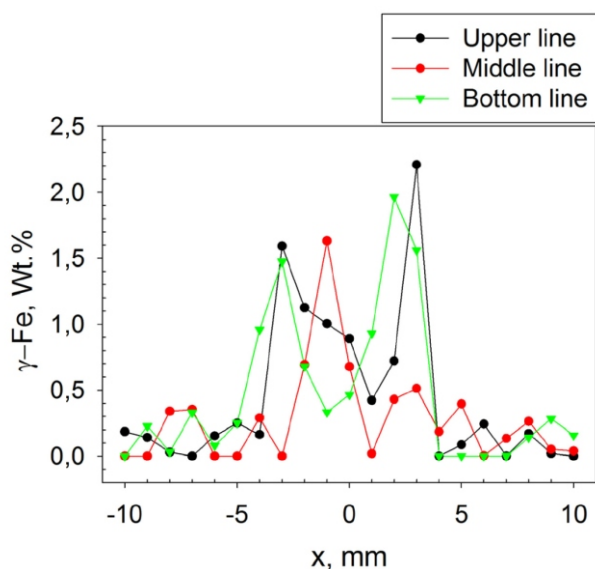


Figure 2. Weight percentage of retained austenite for laser weld.

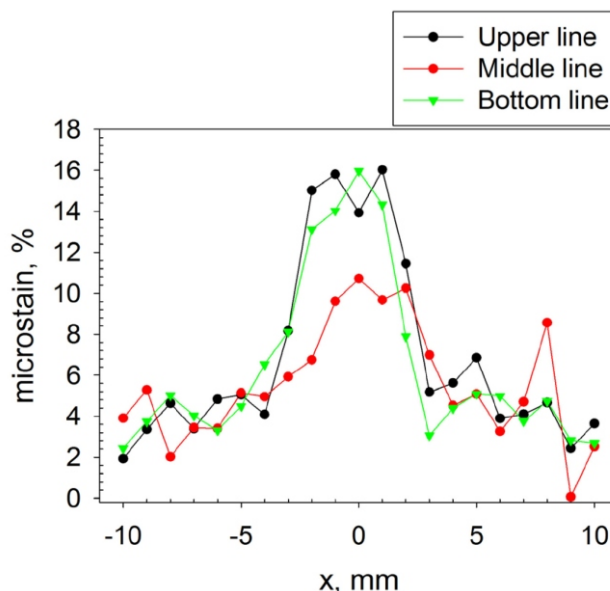


Figure 3. Microstrain for laser weld.

Measurements were carried out at the CANAM infrastructure of the NPI ASCR Řež supported through MŠMT project No. LM2011019 and Czech Science Foundation GAČR through the project No. 14-36566G entitled as Multidisciplinary Research Centre for Advanced Materials. The authors thank to Doc. Němeček for supplying the

laser weld. This work was supported by the Student Grant Competition CTU in Prague grant No. SGS16/245/OHK4/3T/14.

Session II

S5

Damage of Crystal Structure of Galenites by Radiation ^{210}Pb

POŠKOZENÍ KRystalOVÉ STRUKTURY GALENITŮ RADIOAKTIVNÍM ZÁŘENÍM ^{210}Pb

M. Čurda^{1,2}, V. Goliáš¹, M. Klementová³, L. Strnad⁴, Z. Matěj⁵, R. Škoda⁶

¹Ústav geochemie, mineralogie a nerostných zdrojů, Přírodovědecká fakulta, Univerzita Karlova, Albertov 6, 128 43 Praha 2

²Česká geologická služba, Geologická 6, 152 00 Praha 5

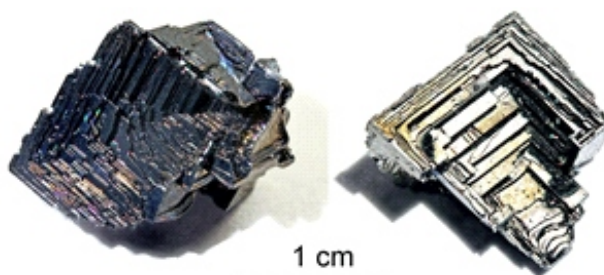
³Ústav anorganické chemie, Akademie věd České republiky, 250 68 Husinec-Řež

⁴Laboratoře geologických ústavů, Přírodovědecká fakulta, Univerzita Karlova, Albertov 6, 128 43 Praha 2

⁵Katedra fyziky kondenzovaných látek, Matematicko-fyzikální fakulta, Univerzita Karlova, Ke Karlovu 5, 121 16 Praha 2

⁶Ústav geologických věd, Masarykova Univerzita, Kotlářská 2, 611 37 Brno
michalcurda@centrum.cz

Studované vzorky novotvořených galenitů pocházejí z hořících hald po těžbě černého uhlí a uranu z Radvanic, Markoušovic a Rybníčku (okres Trutnov). Haldový materiál zde obsahoval velké množství uhelného materiálu obohaceného o uran. Při hoření haldového materiálu se Pb, včetně jeho izotopu ^{210}Pb , dostává do unikajících plynů. Při následné desublimaci a krystalizaci galenitů vstupuje do jejich krystalových struktur. Radioaktivita studovaných galenitů je tak způsobena přítomností izotopu ^{210}Pb , jeho dceřinými rozpadovými produkty (^{210}Bi a ^{210}Po) a sekundárními jadernými efekty způsobenými vysokou beta



Obrázek 1. Kostrovité krystaly galenitu z Radvanic.